J. Phys.: Condens. Matter **10** (1998) 2933–2945. Printed in the UK PII: S0953-8984(98)89803-2

Structural stability of YM_2 compounds (M = Al, Ni, Cu) studied by *ab initio* total-energy calculations and high-pressure x-ray diffraction

A Lindbaum†, J Hafner‡, E Gratz† and S Heathman§

† Institute for Experimental Physics, Vienna University of Technology, Wiedner Hauptstrasse 8-10/131, A-1040 Wien, Austria

‡ Institute for Theoretical Physics and Centre for Computational Materials Science, Vienna University of Technology, Wiedner Hauptstrasse 8-10/136, A-1040 Wien, Austria

§ European Commission, Joint Research Centre, Institute for Transuranium Elements, Postfach 2340, D-76125 Karlsruhe, Germany

Received 5 December 1997

Abstract. A combination of *ab initio* total-energy calculations and high-pressure x-ray diffraction experiments has been used to study the phase stability of Y-based 1:2 compounds. The motivation for these investigations was to clarify the origin of the change of the structure among the YT_2 compounds (T = 3d transition element) between the neighbouring elements Ni (YNi_2: defect superstructure of cubic Laves phase C15) and Cu (YCu_2: orthorhombic $CeCu_2$-type structure). As a test of the *ab initio* calculations the cubic YAl_2 Laves phase compound has been included in the investigations.

The *ab initio* calculations confirm the reversal of the relative stabilities of the $CeCu_2$ and C15 phases in YCu_2 and YNi_2 and give also the correct results for YAl_2. Furthermore a pressure-induced structural transition is predicted for YCu_2.

The high-pressure x-ray experiments show that there is very good agreement between the calculated and the measured pressure dependence of the lattice parameters of YCu_2 up to about 10 GPa. Above 10 GPa the structure starts to become irreversibly amorphous. This instability may be a hint at the structural phase transition predicted by the calculations.

1. Introduction

Among the YT_2 series (T = 3d transition metal) there is a change of the stable crystal structure between the two neighbouring 3d elements Ni and Cu. YMn_2, YFe_2, YCo_2 and YNi_2 show the cubic Laves phase (C15) structure, whereas YCu_2 and YZn_2 crystallize in the completely different orthorhombic $CeCu_2$-type structure (see for instance [1]). However, it should be noted that YNi_2 does not crystallize in the ideal C15 structure but in a superstructure of C15 with ordered vacancies at the Y sites [2, 3], which is very similar to the C15 structure. The C15 structure has cubic symmetry with no free internal parameters, whereas the $CeCu_2$ structure is orthorhombic and has three atomic positions not fixed by the symmetry (z_{Ce}, y_{Cu}, z_{Cu}).

The aim of the present work is to investigate the origin of the above-mentioned change of the structure among the YT_2 series. For that purpose *ab initio* total-energy calculations as well as high-pressure x-ray diffraction experiments were performed.

0953-8984/98/132933+13$19.50

The aim of the *ab initio* calculations is to determine the energy differences between the $CeCu_2$-type and C15-type structures for the compounds YNi_2 and YCu_2, i.e. it should be clarified whether the theory confirms that for YCu_2 the $CeCu_2$ structure is stable while for YNi_2 the C15 structure is energetically favourable. YAl_2 should serve as a 'test compound' for the *ab initio* calculations (Al is the only non-d-transition element forming the C15 structure with Y).

For YCu_2 high-pressure x-ray diffraction experiments using synchrotron radiation and a diamond anvil cell were performed with two objectives: (i) the question of a possible structural transition under pressure should be answered and (ii) the pressure dependence of the lattice parameters of this orthorhombic compound should be compared with the *ab initio* calculations.

2. Experimental and theoretical background

2.1. Ab initio total-energy calculations

Ab initio calculations of the total energy and of the electronic structure were performed using the Vienna *ab initio* simulation package VASP [4, 5]. VASP performs an iterative solution of the Kohn–Sham equations of local-density-functional (LDF) theory based on residuum-minimization and optimized charge-density mixing routines [5] and allows us to use generalized gradient corrections. In the present calculations we use the exchange–correlation functional based on the quantum Monte Carlo calculations of Ceperley and Alder, as parametrized by Perdew and Zunger [6] and the gradient corrections proposed by Perdew *et al* [7]. The electronic eigenstates are expanded in terms of plane waves; the electron–ion interaction is described in terms of ultrasoft pseudopotentials [8, 9]. VASP allows for the calculations of the Hellmann–Feynman forces acting on the atoms and of the stresses on the unit cell. Hence the total energy may be optimized with respect to the volume and shape of the unit cell and to the positions of the atoms within the cell, with no other restrictions than those imposed by space-group symmetry. For Brillouin-zone (BZ) integrations we used the Methfessel–Paxton technique [10] with a modest smearing of the one-electron levels. Convergence of the results with respect to the $\boldsymbol{k}$-point mesh for BZ integrations, the fast-Fourier-transform meshes used for the representation of the wave-functions, charge densities and potentials, and with respect to the cut-off energy of the plane-wave basis set, was carefully tested. For total-energy calculations a $5 \times 5 \times 5$ $\boldsymbol{k}$-point mesh was found to be sufficient; a finer mesh was used for calculating the electronic density of states. For all other technical details we refer to [5].

While for transition metals with a nearly full d-band ultrasoft pseudopotentials allow us to achieve convergence with respect to the plane-wave basis set at a modest cut-off energy of 150 to 200 eV [9], special problems arise for transition metals with only partially filled d bands such as Y. Total-energy calculations for pure Y show that without generalized gradient corrections (GGCs) the equilibrium atomic volume (V_Y(exp) = 32.98 Å^3 at 0 K) is strongly underestimated (V_Y(LDA) = 29.5 Å^3), even if the Y 4p 'semicore states' are treated as valence electrons (V_Y(4p LDA) = 30.1 Å^3). The best prediction for the equilibrium atomic volume is achieved with GGC and treating the Y 4p states as valence electrons: V_Y(4p GGC) = 32.80 Å^3. For these reasons throughout this study GGCs are used and the Y 4p states are treated as valence electrons. Details of the construction of the Y pseudopotentials have been given in [11].

2.2. High-pressure diffraction experiments

The experimental studies were performed at the x-ray diffraction beamline at the synchrotron ELETTRA (Trieste, Italy) with an angle dispersive detector system (image plate) and at the F3 beamline of storage ring DORIS III of HASYLAB (synchrotron DESY, Hamburg, Germany) using an energy dispersive detector system. The measurements were made at room temperature on a powdered polycrystalline YCu_2 sample using a Syassen–Holzapfel-type diamond anvil cell [12]. Microsamples of the material were loaded into a 0.2 mm hole drilled into an annealed (800 °C for 3 hours) and pre-indented Inconel X750 gasket along with quartz powder [13] (at ELETTRA) or a ruby splinter (at HASYLAB) for pressure determination. A 4:1 methanol–ethanol mixture and silicone oil were used as the pressure-transmitting media.

3. Results and discussion

3.1. Crystal structures

The $MgCu_2$-type (C15) and the $CeCu_2$-type crystal structures belong to the most common AB_2 structures [14]. The cubic C15 structure (space group $Fd3m$) belongs to a family of tetrahedally close-packed structures known as Laves phases. The smaller B atoms form a network of face- and corner-sharing tetrahedra, the larger A atoms are accommodated in the large holes of this network. In the C15 structure the sublattice of the A atoms has a diamond structure; the primitive cell contains two formula units with all atomic sites uniquely determined by symmetry. The stability of Laves phases is thought to be determined by packing arguments, the relative stability of the different stacking variants depending on the degree of filling of the valence band [15]. Ideal space filling is achieved at a radius ratio of $R_A/R_B = 1.225$, but it is well known that quantum-chemical effects can lead to a 'chemical compression' of the usually more electropositive A atom so that compounds with a nominal radius as large as $R_A/R_B \approx 1.4$ can be stable [15].

The orthorhombic $CeCu_2$ structure (space group *Imma*) may be viewed as a compact three-dimensional arrangement of slightly distorted trigonal prisms centred by the smaller atoms. The primitive unit cell contains two formula units; there are three atomic position parameters not fixed by the symmetry (details see below). $CeCu_2$-type phases exist mainly in compounds where the dominant factor seems to be the large radius ratio R_A/R_B (e.g. $CaZn_2$: $R_{Ca}/R_{Zn} = 1.48$, calculated in terms of the Goldschmidt radii). A transition from stable Laves to stable $CeCu_2$ structures is not only found in the YT_2 series, but also in the series of homovalent alkaline-earth compounds (C14-type $CaMg_2$: $R_{Ca}/R_{Mg} = 1.23$ and $CeCu_2$-type $CaZn_2$: $R_{Ca}/R_{Zn} = 1.48$). However, whereas in the $CaMg_2 \rightarrow CaZn_2 \rightarrow CaCd_2$ series with a free-electron-like band-structure around the Fermi level the size effect is the most important factor determining the phase stability, the larger radius ratio of YNi_2 ($R_Y/R_{Ni} = 1.448$) compared to YCu_2 ($R_Y/R_{Cu} = 1.413$) demonstrates that in this case the explanation for the C15→$CeCu_2$ transition can be found only in electronic effects superseding the size effect.

The higher packing achieved in the C15 structure suggests the possibility of a pressure-induced $CeCu_2$ →C15 transition. However, we have to note that because of the pronounced differences between the two structures no simple transformation path exists and the mechanism of such a transition is probably a diffusive one.

3.2. Phase stability and phase transition in YCu_2

In figure 1 the calculated total energy as a function of the volume of the primitive unit cell is shown for both the C15- and the $CeCu_2$-type structures (for both, the primitive unit cell contains two formula units). The difference between the equilibrium (minimum) energies of the two structures ΔE(C15–$CeCu_2$) is +0.36 eV per formula unit, i.e. the fact that YCu_2 crystallizes in the $CeCu_2$ structure is confirmed by the *ab initio* total-energy calculations. It is interesting to note that the predicted equilibrium (minimum-energy) volume is smaller for the C15 structure, i.e. the packing would be more compact for C15, nevertheless the $CeCu_2$ structure is energetically favourable.

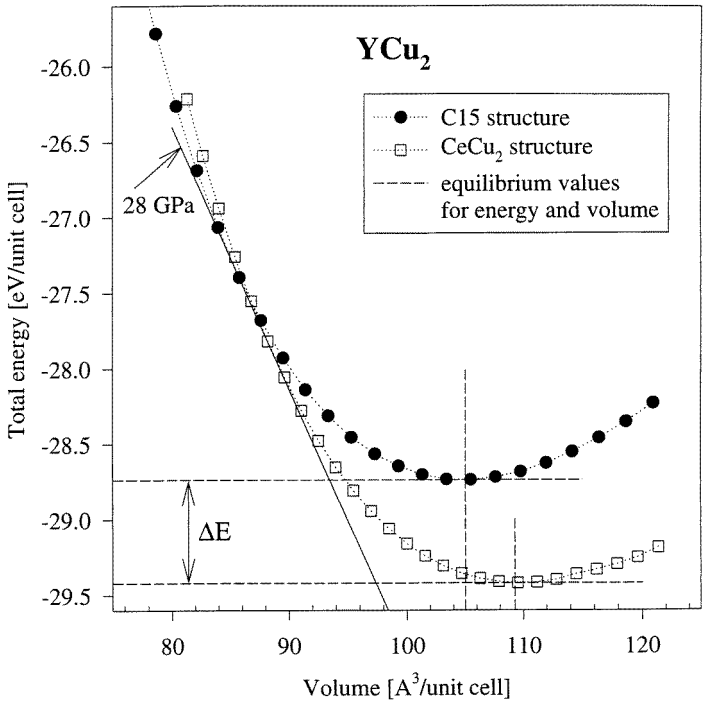

Figure 1. Total energy against volume for YCu_2 in the $CeCu_2$ and C15 structures.

The crossing of the energy–volume curves of the two structures at roughly 87 $Å^3$ shows that the C15 structure is energetically favourable at very high pressures, i.e. there should be a pressure-induced phase transition from the $CeCu_2$ to the C15 structure at roughly 28 GPa (this can be estimated from the slope of the common tangent to the two energy–volume curves). But note that it is also possible that there are one or more other structures which become energetically favourable at pressures lower than 28 GPa, i.e. from the comparison with the C15 structure alone it only follows that there must be some structural transition of the $CeCu_2$ structure at a pressure not higher than 28 GPa.

The energy-dispersive high-pressure synchrotron measurements of YCu_2 up to 30 GPa show that above about 10 GPa the sample starts to become irreversibly amorphous. As illustration a part of the diffraction patterns at 0 and 19 GPa is shown in figure 2. The amorphization might be a hint at the predicted phase transition. Maybe room temperature at which the experiments were performed is too low for a diffusion-limited $CeCu_2 \rightarrow$ C15

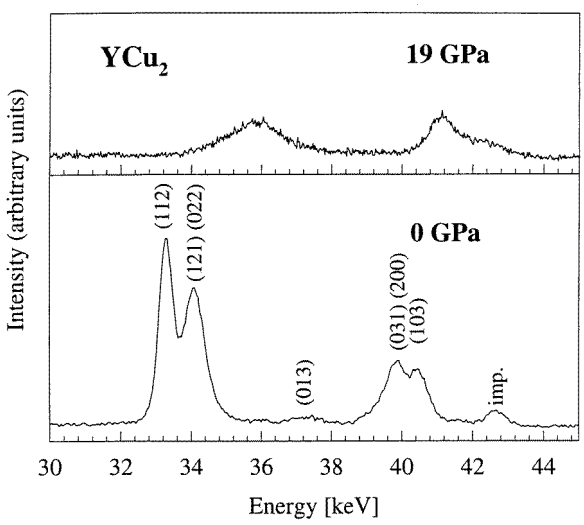

Figure 2. Energy-dispersive diffraction patterns of YCu_2 at 0 and 19 GPa.

transition to be completed during the time the sample was exposed to high pressure. It should be mentioned that the same effect was observed with $GdCu_2$ and $NdCu_2$ samples. These compounds also crystallize in the $CeCu_2$ structure.

In table 1 the experimental and calculated values of the lattice constants *a*, *b*, *c* and the atomic position parameters y_{Cu}, z_{Cu} and z_Y of YCu_2 at ambient pressure ($P = 0$ GPa) are compared (y_{Cu}, z_{Cu} and z_Y are not fixed by the structural symmetry). The experimental values for *a*, *b* and *c* are taken from the extrapolation of low-temperature thermal expansion measurements to $T = 0$ K [16]. The experimental values for y_{Cu}, z_{Cu} and z_Y show no significant change between room temperature and 4 K; they are taken from [17].

Table 1. Experimental and calculated values of the lattice constants a, b, c and of the atomic position parameters y_{Cu}, z_{Cu} and z_Y of YCu_2 (the experimental values are taken from an extrapolation to $T = 0$ K).

	Ab initio calculation	Experiment	Deviation
a [Å]	4.284	4.296 ± 0.001	−0.3%
b [Å]	6.923	6.841 ± 0.003	1.2%
c [Å]	7.368	7.268 ± 0.001	1.4%
z_Y	0.544	0.544 ± 0.002	< 0.001
y_{Cu}	0.053	0.050 ± 0.002	0.003
z_{Cu}	0.165	0.162 ± 0.002	0.003

In figure 3 the results of the *ab initio* calculation are compared with the pressure dependence of the lattice parameters determined by the angle-dispersive high-pressure x-ray diffraction measurements up to 9 GPa (the resolution of the energy-dispersive measurements was not good enough to determine the orthorhombic lattice parameters with the same accuracy). To make the comparison easier the values are normalized to the values at 0 GPa. Within the accuracy of the experimental values there is very good agreement between theory and experiment. The deviation of the absolute values of the lattice parameters (see table 1) is smaller than 1.5% for all parameters.

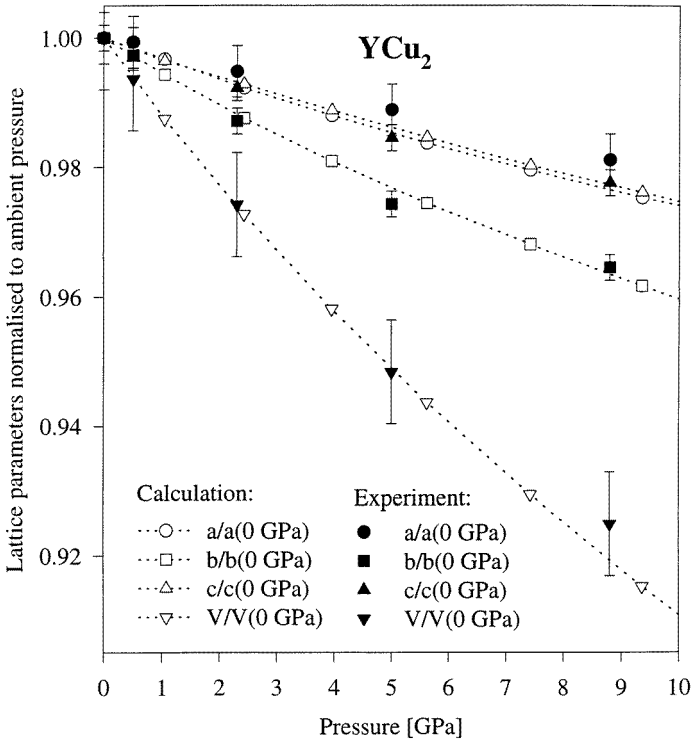

Figure 3. Comparison of experimental and calculated pressure dependences of the lattice parameters of YCu_2.

3.3. Phase stability of YNi_2 and YAl_2

In figures 4 and 5 the results of the total-energy calculations for YNi_2 and YAl_2 in the C15 and the $CeCu_2$ structures are shown. In contrast to YCu_2 the C15 structure is energetically favourable for these two compounds: ΔE(C15–$CeCu_2$) is -0.07 eV fu^{-1} for YNi_2 and -0.04 eV fu^{-1} for YAl_2. Again the predicted equilibrium (minimum) volume is smaller for the C15 structure (the structure with the higher packing efficiency).

In table 2 the experimental and calculated values of the cubic lattice parameter at ambient pressure ($P = 0$ GPa) are compared. The experimental values are taken from the extrapolation of low-temperature thermal expansion measurements to $T = 0$ K [18, 19]. The lattice parameter is slightly overestimated for both compounds; however the deviation is smaller than 1%.

Table 2. Experimental and calculated lattice constants for C15-type YNi_2 and YAl_2.

	Ab initio calculation	Experiment (Å)	Deviation (%)
YNi_2	7.227	7.161 ± 0.001	0.9
YAl_2	7.895	7.847 ± 0.001	0.6

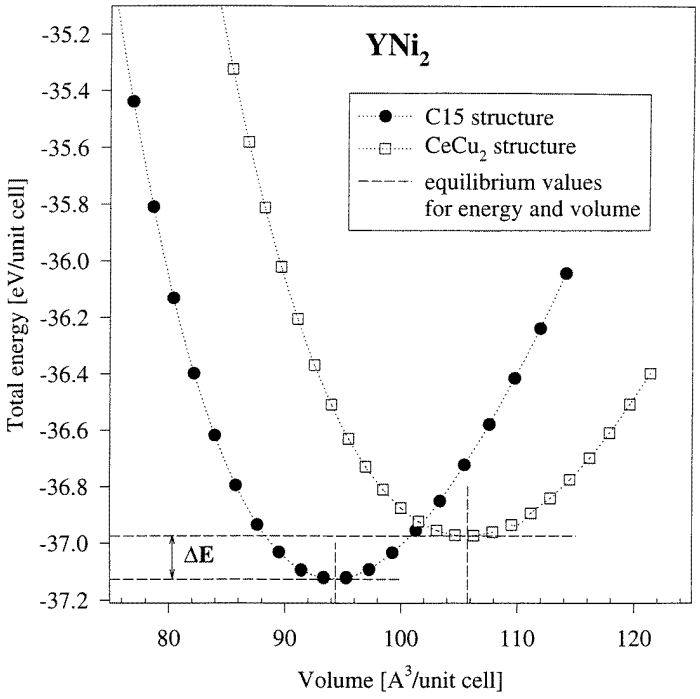

Figure 4. Total energy against volume for YNi_2 in the $CeCu_2$ and C15 structures.

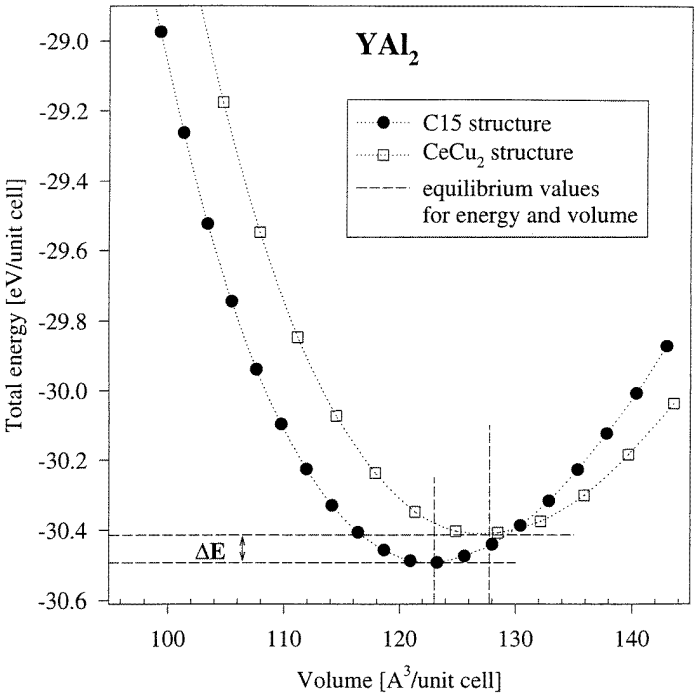

Figure 5. Total energy against volume for YAl_2 in the $CeCu_2$ and C15 structures.

A further result of the *ab initio* calculation is that in the case of the $CeCu_2$ structure for both compounds YNi_2 and YAl_2 the atomic position parameters z_Y, $y_{Ni/Al}$ and $z_{Ni/Al}$ relax to $z_Y = 0.5000\ldots(=1/2)$, $y_{Ni/Al} = 0.0000\ldots(=0)$ and $z_{Ni/Al} = 0.1666\ldots(=1/6)$, and the c/a ratio relaxes to values which differ by less than 0.3% from $\sqrt{3}$, i.e. the $CeCu_2$ structure relaxes to a high-symmetry hexagonal structure, which can be described within the space group *P6/mmm* with Y on 1a sites and Ni/Al on 2d sites, i.e. as the AlB_2 structure (C32). This is a further hint that the $CeCu_2$ structure cannot be stable in the case of YNi_2 and YAl_2. For YCu_2 (see table 1) and for all RCu_2 also crystallizing in the $CeCu_2$ structure [20] the three free atomic position parameters and the c/a ratio are significantly different from 1/2, 0, 1/6 and $\sqrt{3}$, respectively.

We also note that the close relationship between the $CeCu_2$ and the AlB_2 structures is well established. In $CaHg_2$ both structures are realized as high- and low-temperature polytypes and AlB_2 is also the stable crystal structure of $LaCu_2$ [14].

3.4. Formation enthalpy and volume

From the calculated ground-state properties of the intermetallic compounds and of the pure metals, the heat of formation $\Delta H = E(YT_2) - E(Y) - 2E(T)$ and the volume of formation $\Delta V = V(YT_2) - V(Y) - 2V(T)$ may be calculated. The results are compared in table 3. For YCu_2 and YNi_2 the comparison with the calorimetric measurements of Watanabe and Kleppa [21] and Colinet *et al* [22] shows that the *ab initio* calculations consistently overestimate the heat of formation. We note that on the other hand there is a very good agreement of the *ab initio* results with the predictions of the empirical model of Miedema [23]: $\Delta H(YCu_2) = -0.99$ eV fu^{-1}, $\Delta H(YNi_2) = -1.40$ eV fu^{-1}. This is just a further confirmation of the fact that—although the physical reasoning underlying the model of Miedema may not be correct (see e.g. the critique formulated by Pettifor [24])—this model represents an astonishingly accurate parametrization of the density-functional predictions.

Table 3. Total energy, equilibrium volume, heat and volume of formation of the pure elements and intermetallic compounds (per formula unit, experimental values given in parentheses).

	E [eV]	V [Å^3]	ΔH [eV]	$\Delta V/V$ [%]
Y	−6.259	32.80 (32.98)[a]	—	—
Cu	−3.759	12.08 (11.70)[a]	—	—
Ni	−5.420	11.00 (10.86)[a]	—	—
Al	−3.670	16.60 (16.39)[a]	—	—
YCu_2	−14.69	54.63 (53.40)[b]	−0.91 (−0.63)[c]	−4.1 (−5.3)
YNi_2	−18.55	47.18 (45.90)[d]	−1.45 (−1.21)[e]	−13.9 (−16.1)
YAl_2	−15.25	61.51 (60.40)[d]	−1.64	−6.8 (−8.2)

[a] From extrapolations of thermal expansion measurements to $T = 0$ K [25].
[b] From extrapolations of thermal expansion measurements to $T = 0$ K [16].
[c] Calorimetric measurements [21].
[d] From extrapolations of thermal expansion measurements to $T = 0$ K [18, 19].
[e] Calorimetric measurements [22].

A characteristic feature of all YT_2 compounds studied here is a rather large volume contraction. The trend in the negative volumes of formation is well predicted by the calculation, but ΔV is consistently slightly underestimated.

Our results demonstrate that the GGC only partially corrects the 'overbinding' of the LDA as far as the energy is concerned; however it really improves the predictions for the equilibrium volumes, especially for the pure metals. For the compounds where the distribution of the electronic density is less homogeneous (and hence the charge-density gradients are larger) the GGC tends to overcorrect the LDA error and this leads to the observed underestimation of the volume of formation.

3.5. Electronic structure of YCu_2 and YNi_2

Figures 6 and 7 show the total, partial and angular-momentum-decomposed electronic densities of states (DOS) for YCu_2 in the $CeCu_2$ and C15 structures, calculated with a $9 \times 9 \times 9$ $\boldsymbol{k}$-point mesh. In both cases the characteristic features are a broad Y 4d band around the Fermi level and a well separated narrower Cu 3d band at energies between 2 and 4 eV below the Fermi level. Compared to pure Cu, the upper edge of the 3d band is shifted to higher binding energies by about 1 eV. The d-band shift is characteristic of the strong covalent d–d interaction in alloys of 'early' transition metals (with a less than half-filled d-band) and 'late' transition or noble metals, as first pointed out by Oelhafen *et al* [26].

The present pseudopotential results agree with earlier calculations of the electronic structure of crystalline YCu_2 and of a series of amorphous Y_xCu_{1-x} alloys [27, 28]. We also refer to [28] for a detailed comparison of electronic structure calculations with photoelectron spectra.

In the present context it is important to note that the width of the Cu 3d band is larger in the $CeCu_2$ than in the C15 structure. Furthermore the Y 4d band shows more structure in the C15 phase, with the Fermi level falling onto a local maximum of the DOS. Both the Cu 3d band broadening and the structure-induced features of the valence band favour the $CeCu_2$ structure.

Figures 8 and 9 show the DOSs calculated for YNi_2 in the C15 and AlB_2 phases (the AlB_2 structure is a special case of the $CeCu_2$ structure, see section 3.3). The important difference between YNi_2 and YCu_2 is that the Ni 3d band is not completely filled and has a much stronger overlap with the Y 4d band. An immediate consequence of the stronger Y 4d–Ni 3d interaction is the formation of a hybridization gap. This pseudogap is particularly pronounced in the $CeCu_2$- (or rather AlB_2-) type phase where it lies 0.5 eV below the Fermi level placing E_F onto a local maximum of the DOS (figure 8). The d–d hybridization is weaker in the C15 phase where the Fermi level falls into a local minimum of the DOS.

Hence the reversal of the relative stabilities of the C15 and $CeCu_2$ phases in YNi_2 and YCu_2 is mainly an electronic effect driven by the structure-induced rearrangements of the one-electron levels. This is supported by a decomposition of the structural energy differences ΔE(C15–$CeCu_2$) into the electrostatic terms (Ewald plus Hartree energies) ΔE_{elst}, the exchange–correlation terms ΔE_{xc} and the contribution from the sum over the one-electron energies ΔE_{1e}, i.e. $\Delta E = \Delta E_{elst} + \Delta E_{xc} + \Delta E_{1e}$. The electrostatic terms always favour the more compact C15 structure: $\Delta E_{elst} = -6.56$ eV fu^{-1} for YCu_2 and $\Delta E_{elst} = -16.60$ eV fu^{-1} for YNi_2. The exchange–correlation and one-electron energies favour the $CeCu_2$ structure: $\Delta E_{xc} = +0.03$ eV fu^{-1} for YCu_2 and $\Delta E_{xc} = +0.34$ eV fu^{-1} for YNi_2, $\Delta E_{1e} = +6.89$ eV fu^{-1} for YCu_2 and $\Delta E_{1e} = +16.19$ eV fu^{-1} for YNi_2, mainly due to the stronger bonding–antibonding splitting (and hence the stronger covalent d–d band) in the $CeCu_2$ structure.

Concerning YNi_2 it is also important to note that in the $CeCu_2$ (AlB_2) phase the Y atoms form trigonal prisms centred by the Ni atoms. This trigonal-prismatic coordination of Ni by Y exists also in the Y-rich intermetallic Y–Ni compounds Y_3Ni (Ti_3Ni type), Y_3Ni_2 and YNi

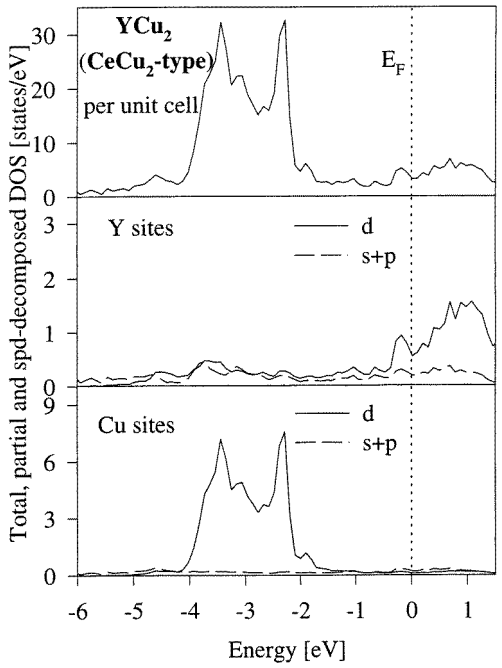

Figure 6. Calculated total, partial and angular-momentum-decomposed DOS of YCu_2 ($CeCu_2$ structure).

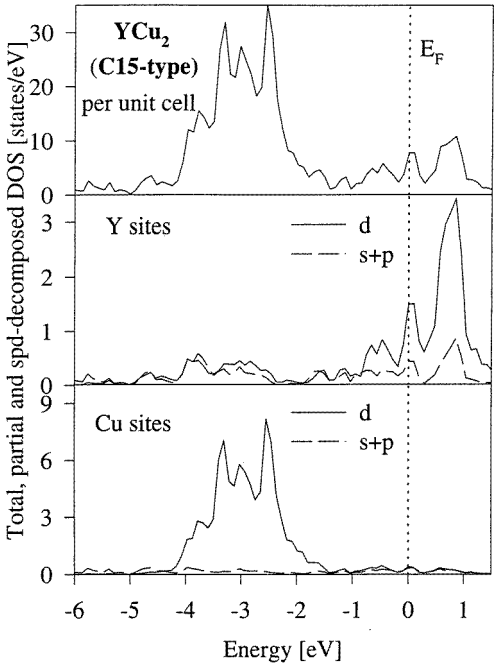

Figure 7. Calculated total, partial and angular-momentum-decomposed DOS of YCu_2 (C15 structure).

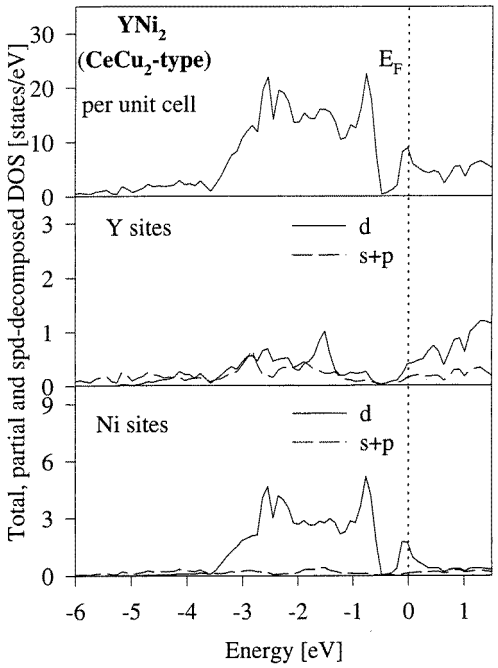

Figure 8. Calculated total, partial and angular-momentum-decomposed DOS of YNi_2 ($CeCu_2$ structure).

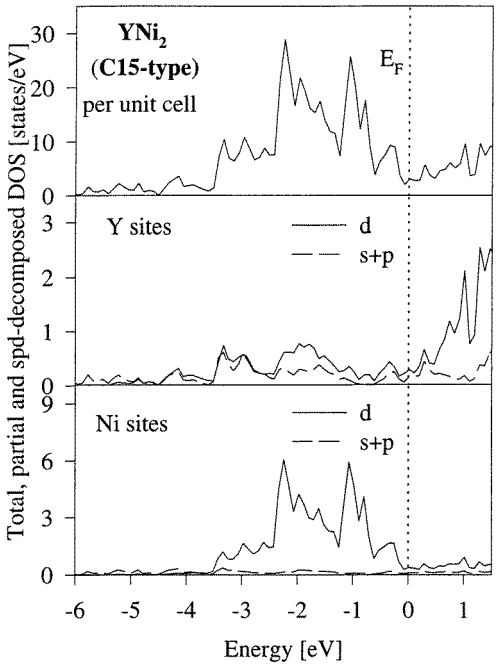

Figure 9. Calculated total, partial and angular-momentum-decomposed DOS of YNi_2 (C15 structure).

(FeB type) where the trigonal prisms are more loosely packed (only face or edge sharing, in contrast to the compact space-filling arrangement in $CeCu_2$ and AlB_2 structures). The local trigonal-prismatic order is also preserved in the amorphous Y_xNi_{1-x} ($x \sim 0.67$) phases [29]. All the trigonal-prismatic crystalline and amorphous Y–Ni phases are characterized by pronounced hybridization-induced minima in the DOS [28, 29]. In contrast at the Ni-rich end of the phase diagram tetrahedrally close-packed Frank–Kasper phases are stable (Y_2Ni_{17}, YNi_5, YNi_4,Y_2Ni_7, YNi_3 and YNi_2)—see [29] for a more detailed discussion. The weaker chemical order in the Frank–Kasper phases is reflected by less pronounced hybridization-induced features in the electronic DOS. The phase diagrams of other Y–T systems (with T from the end of the 3d series) have a similar character.

Hence the C15→ $CeCu_2$ transition in the series of YT_2 compounds as well as the competition between trigonal-prismatic and tetrahedally close-packed phases may be understood in terms of the competition between space-filling and electronic effects.

4. Summary and conclusion

(i) Our *ab initio* LDF calculations confirm that YCu_2 should show the $CeCu_2$ structure, while for the neighbouring compound YNi_2 the C15 structure should be energetically favourable, i.e. the change of the stable crystal structure of the YT_2 compounds between T=Ni and T=Cu is in agreement with theory. This reversal of the stabilities is entirely due to electronic effects. The calculations for YAl_2 which were made in order to test the model on a simpler system gives also the correct results. GGCs are important for achieving accurate predictions of the equilibrium densities.

(ii) The *ab initio* calculations for the pressure dependence of the lattice parameters of YCu_2 agree very well with the high-pressure x-ray diffraction experiments.

(iii) The *ab initio* calculations for YCu_2 show that there might be a phase transition from the $CeCu_2$ to the C15 structure at approximately 28 GPa. The experiments at room temperature only show that the structure starts to become irreversibly amorphous above 10 GPa. Maybe heating of the sample during the high-pressure measurements would allow the atoms to overcome the energy barrier between the $CeCu_2$ and C15 structure. This will be the subject of further investigations.

(iv) As mentioned in the introduction YNi_2 does not show the pure C15 structure but a superstructure of C15 with ordered Y vacancies, which is very similar to the pure C15 structure. Furthermore at about 740 K and ambient pressure an order–disorder phase transition has been observed, i.e. the Y vacancies become disordered. High-pressure experiments showed that this transition also takes place at room temperature and pressures above about 25 GPa [2, 3]. *Ab initio* calculations concerning the stability of the YNi_2 superstructure are the subject of present investigations and will be published soon.

Acknowledgments

This work was supported by the Austrian Science Foundation FWF (project: P-11581-PHY) and the ‘Hochschuljubiläumsstiftung der Stadt Wien’. The authors wish to thank the responsible people at ELETTRA and DESY (HASYLAB) for the fruitful co-operation, A Lahner who was responsible for the building of the high-pressure diamond anvil cell and R Miletich for many important hints concerning the sample preparation with our high-pressure diamond anvil cell.

References

[1] Villars P and Calvert L D 1985 *Pearson's Handbook of Crystallographic Data for Intermetallic Phases* (Materials Park, OH: American Society for Metals)
[2] Latroche M, Paul-Boncour V, Percheron-Guegan A and Achard J C 1990 *J. Less-Common Met.* **161** L27
[3] Gratz E, Kottar A, Lindbaum A, Mantler M, Latroche M, Paul-Boncour V, Acet M, Barner Cl, Holzapfel W B, Pacheco V and Yvon K 1996 *J. Phys.: Condens. Matter* **8** 8351
[4] Kresse G and Hafner J 1993 *Phys. Rev.* B **48** 13 115
Kresse G and Hafner J 1994 *Phys. Rev.* B **49** 14 251
[5] Kresse G and Furthmueller J 1996 *Comput. Math. Sci.* **6** 15
Kresse G and Furthmueller J 1996 *Phys. Rev.* B **55** 11 961
[6] Perdew J P and Zunger A 1981 *Phys. Rev.* B **23** 5048
[7] Perdew J P, Chevary J A, Vojsko S H, Jackson K A, Pedersen M R, Singh D J and Fiolhais C 1992 *Phys. Rev.* B **46** 6671
[8] Vanderbilt D 1990 *Phys. Rev.* B **41** 7892
[9] Kresse G and Hafner J 1994 *J. Phys.: Condens. Matter* **6** 8245
[10] Methfessel M and Paxton A T 1989 *Phys. Rev.* B **40** 3616
[11] Magaud L, Pasturel A, Kresse G and Hafner J 1997 *Phys. Rev.* B **55** 13 479
[12] Syassen K and Holzapfel W B 1975 *Europhys. Conf. Abstr.* **1A** 75–6
[13] Angel R J, Allan D R, Miletich R and Finger L W 1997 *Appl. Crystallogr.* **30** 461–6
[14] Villars P 1989 *The Structures of Binary Compounds* ed F R de Boer and D G Pettifor (Amsterdam: North-Holland)
[15] Hafner J 1989 *The Structures of Binary Compounds* ed F R de Boer and D G Pettifor (Amsterdam: North-Holland)
[16] Gratz E, Rotter M, Lindbaum A, Mueller H, Bauer E and Kirchmayr H 1993 *J. Phys.: Condens. Matter* **5** 567
[17] Lindbaum A 1991 *Diploma Thesis* Technische Universität Wien, Institut für Experimentalphysik
[18] Gratz E and Lindbaum A 1994 *J. Magn. Magn. Mater.* **137** 115
[19] Lindbaum A 1994 *PhD Thesis* Technische Universität Wien, Institut für Experimentalphysik
[20] Debray D 1973 *J. Less-Common. Met.* **30** 237
[21] Watanabe S and Kleppa O J 1984 *Metall. Trans.* B **15** 357
[22] Colinet C, Pasturel A and Buschow K H J 1987 *J. Appl. Phys.* **62** 3712
[23] de Boer F R, Boom R, Mattens W C M, Miedema A R and Niessen A K 1988 *Cohesion in Metals* ed F R de Boer and D G Pettifor (Amsterdam: North-Holland)
[24] Pettifor D G 1987 *Solid State Physics Advances in Research and Applications* vol 40, ed H Ehrenreich and D Turnball (New York: Academic) p 1
[25] Touloukian Y S, Kirby R K, Taylor R E and Desai P D 1976 *Thermal Expansion—Metallic Elements and Alloys* (New York: Plenum)
[26] Oelhafen P 1983 *Glassy Metals II* ed H Beck and H J Güntherodt (Berlin: Springer)
[27] Harima H and Yanase A 1992 *J. Phys. Soc. Japan* **61** 602
[28] Hausleitner Ch, Tegze M and Hafner J 1992 *J. Phys.: Condens. Matter* **4** 9557
[29] Hausleitner Ch and Hafner J 1992 *Phys. Rev.* B **45** 128